# Mechanistic Study of plasmon assisted *in situ* photoelectrochemical CO<sub>2</sub> reduction to acetate with a Ag/Cu<sub>2</sub>O nanodendrite electrode

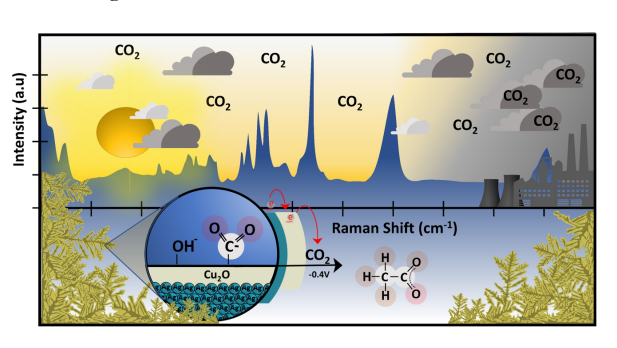
Esteban Landaeta<sup>1#</sup>; Nir I. Kadosh<sup>1</sup>; Zachary D. Schultz<sup>1\*</sup>

- <sup>1</sup> Department of Chemistry and Biochemistry, The Ohio State University, Columbus, OH 43210, USA
- \* corresponding author email: schultz.133@osu.edu

#current address: Escuela de Ingeniería, Universidad Central de Chile, Santiago, Chile

## **Abstract**

Electrochemical and more recently, photoelectrochemical  $CO_2$  reduction have been widely investigated to convert atmospheric  $CO_2$  into other useful chemicals. However, understanding the mechanism and selectivity of materials capable of reducing  $CO_2$  remains a challenge. Using plasmonic dendritic electrodes of silver and cuprous oxide (Ag/Cu<sub>2</sub>O) and employing Raman spectro-electrochemistry (Raman E-CHEM) detection we observe the selective photoelectroreduction mechanism from  $CO_2$  to acetate as a value-added compound instead of the more commonly reported products



like methanol, ethylene, or ethane. The selectivity, efficiency and low overpotential (-0.4V vs Ag/AgCl) in the CO<sub>2</sub> reduction is favored by the basic microenvironment, the semiconductor properties of the Cu<sub>2</sub>O and the accumulation of hot electrons from the Localized Surface Plasmon Resonance (LSPR) of the Ag nanostructure. Lateral surface interactions between adsorbed CO species are key to the formation of acetate. The rate-determining step of the reaction is the single transfer of an electron from the electrode to the CO<sub>2</sub> molecule to reduce it to the \*CO<sub>2</sub><sup>-</sup> radical anion and subsequently forms adsorbed CO, which is a key intermediate in the formation of the carbon-carbon bond during the reduction process.

Keywords: CO<sub>2</sub> reduction, plasmonics, heterogeneous catalysis, photo- electrocatalysis, nanomaterials.

# Introduction

The reduction of CO<sub>2</sub> into added value compounds remains a topic of high interest. In the last decades CO<sub>2</sub> emission has increased over 400 ppm and is considered the main cause of climate change, above other greenhouse gases such as methane, nitrous oxides, water and organofluorocarbons.<sup>1</sup>

 $CO_2$  reduction to  $C_1$ ,  $C_2$  and  $C_{2+}$  compounds is a very important issue due to the fact that these compounds can be useful as fuels, chemical products or chemical precursors. Industrial synthesis of  $C_2$  and  $C_{2+}$  products is more complicated than for  $C_1$  compounds as the development of electrode materials with high selectivity toward these products has been a challenge and, in addition to being complex, has not been studied as in-depth as the formation of  $C_1$  compounds.

Among the metals used for CO2 reduction, Cu has shown the capability to electrochemically reduce CO2 toward hydrocarbons and oxygenates.4 In the early 1980s, Hori and coworkers,<sup>5,6</sup> using a polycrystalline Cu electrode detected mostly CH<sub>4</sub>, C<sub>2</sub>H<sub>4</sub> and HCOO-. More recently, Jaramillo et al detected at least 16 reduction products including methane, ethanol, acetate and carbon monoxide among others7. These products highlight the complexity of this reaction. Interestingly, derived copper oxides have improvements in selectivity towards C2 and oxygenates with the detection of methane, acetylene, and ethanol as the main products.<sup>8,9</sup> It has been further shown with these products that the selectivity towards the C-C coupling is strongly influenced

by the formation of \*CO (asterisk (\*) denotes an adsorbed species) adsorbed on the electrode,<sup>10</sup> since the adsorbed CO decreases the available sites for HER increasing efficiency towards the reduction of CO<sub>2</sub>.<sup>11</sup>

In a recent work, 12 we designed a high surface area silver nanodendrite electrode covered with a copper oxide thin film that can reduce CO2 photoelectrochemically at low overpotential (-0.4V versus Ag/AgCl) in a 0.1M Na<sub>2</sub>SO<sub>4</sub> solution. With the Silver/Copper oxide nanodendrite electrode, we detected a C2 oxygenated compound (Acetate) with a high faradaic efficiency (54%) and interestingly, we detected CO in low quantities with an efficiency of less than 1% giving us a first indication of the pathways by which CO2 is reduced to acetate. Our system showed, not only the C-C coupling at a low overpotential, but also the suppression of the formation of other compounds such as ethylene, ethane, and ethanol. The selectivity and high efficiency at a low overpotential are the result of the plasmonic and semiconductors properties of the Ag/Cu<sub>2</sub>O nanodendrites which helps the electron transfer from the silver nanodendrite to the surface of the electrode to be injected into the LUMO of CO<sub>2</sub>. This plasmonic effect has been highly studied<sup>13–15</sup> and, demonstrated in catalytic processes such as hydrogen electroreduction or oxygen evolution reaction where the necessary overpotential decreases dramatically when the processes occur on a plasmonic material that leads to locally enhanced negative electric fields. 16,17

On the other hand, the role of the Cu<sub>2</sub>O toward the CO<sub>2</sub> reduction has been well described in the literature. Under visible light illumination the band-gap excitation and

formation of free charge carriers is followed by several pathways of de-excitation where, in the best case, the successful donation of the electron to the CO<sub>2</sub> at the surface will lead to the desired reduction reaction. In the case of the Silver-cuprous oxide material, the Fermi level moves upwards, with its potential becoming more negative and then discharging the electrons into the CO<sub>2</sub> more easily than on the Cu<sub>2</sub>O by itself.

Understanding of the CO<sub>2</sub> reduction mechanism is multistep. In addition to the injection of electrons from the electrode, the chemical pathways involve electrons, protons, the cleavage of C-O bonds, and the formation of C-H bonds; all of which are difficult to track while the reaction is ongoing. In recent years, in situ Raman Spectroscopy has offered insight into the nature of the chemical species formed, improving the spectroscopic task of identifying reactants and intermediates while the reaction is ongoing.<sup>19</sup> In these experiments, metal nanomaterials such as Ag, Au and Cu are most commonly used due to the Surface-Enhanced Raman Scattering (SERS) phenomenon. In SERS, when these materials are struck by incident light that matches the localized plasmon resonance of the material, the Raman intensity is enhanced by several orders of magnitude.<sup>20</sup> The SERS signal from silver nanodendrites has provided in situ information from both the electrode and the adsorbates present at the catalytic site. 21,22

The challenge to studying the formation of  $C_2$  products is understanding the formation of the C–C bond as well as the identification of the intermediates that give rise to the final products. In the overall reaction for the reduction of  $CO_2$  to acetate, 8 electrons must be transferred to the  $CO_2$  molecule as shown in equation 1:

$$2CO_2 + 5H_2O + 8\overline{e} \rightarrow CH_3COO^- + 7OH^-$$
 (1)

Considering that the transfer of these 8 electrons is a complex reaction, the combination of in situ SERS and electrochemical measurements is an effective approach to evaluate the chemical species involved and the rate-determining step (RDS) of the reaction meachanism.<sup>23</sup> Thus, in this work we use this approach to elucidate the mechanism of selective photoelectrochemical CO<sub>2</sub> reduction to acetate at low overpotential. The *in situ* Raman, electrochemical and supporting experiments illuminate the identity of key species and identify reaction steps that can be controlled to uniquely alter the products obtained.

# Experimental

### Materials and reagents

Silver nitrate (Sigma Aldrich, >99.0 %), Sodium citrate tribasic dihydrate (Sigma Aldrich, > 99.0%), Copper (II) sulfate pentahydrate (Sigma Aldrich, >98.0%), Sodium Hydroxide (Sigma Aldrich, 97.0 %), and 4-mercaptobenzonitrile (Sigma Aldrich, 95%) were used as received. Ultrapure water (resistivity of 18.2 M $\Omega$ -cm) was used for all aqueous solutions.

#### Electrode modification

The Ag/Cu<sub>2</sub>O electrode was prepared by a double step electrodeposition method (Figure S1). First, the silver nanodendrites electrodeposition was performed using an aluminum foil as working electrode and applying -1.6 V in a

0.05M AgNO<sub>3</sub> solution and then the electrode was dried for 24 hrs. Afterwards, the  $Cu_2O$  was electrodeposited by a multipotential step method in a copper-citrate solution with 0.05 M  $CuSO_4$ · $5H_2O$  and 0.1 M  $C_6H_5Na_3O_7$ · $2H_2O$  ( $Na_3Cit$ ) to then rinsed with ultrapure water as previously described.<sup>24</sup>

#### Electrochemical measurements

Electrochemical and spectroelectrochemical experiments were performed with a CHI 660D potentiostat (CH Instruments, Austin, TX) using a Ag/AgCl (KCl 1M) as a reference electrode and a platinum wire as auxiliary electrode.

To detect products, electrolysis was performed for 1-hour under continuous illumination using a white light LED (Thorlabs) light source (100 Wcm<sup>-2</sup>) and applying -0.4V. While aqueous products were detected by NMR.

Tafel analysis was performed at a scan rate of 10 mVs<sup>-1</sup> in a potential range between +0.2 and -0.3 vs Ag/AgCl (KCl 1M) in a CO<sub>2</sub> saturated 0.1M Na<sub>2</sub>SO<sub>4</sub> solution.

#### Raman spectroelectrochemical measurements

spectroelectrochemical experiments Raman were performed with a Renishaw InVia Microscope equipped with laser and a homemade 632.8 HeNe spectroelectrochemical cell. A Leica 40X (NA =0.80) water immersion objective was used for illumination and collection in these measurements. The photoexcitation of the plasmon was achieved using a 455 nm LED (Thorlabs) as light source. Unlike electrochemical experiments, the use of a 455 LED instead of a white light LED was done to avoid interference with the detected Raman scattering, while exciting the LSPR of the underlying Ag nanostructures. The LED illumination was filtered from the Raman scattering by the 633 edge filter in the Raman microscope used to reject Rayleigh scattering. The LED could be turned on or off to assess photo-induced processes that were analyzed from the data acquired from the surface in the Raman shift range between 110 and 3200 cm<sup>-1</sup>.

### MBN monolayer experiments

A 4-mercaptobenzonitrile (MBN) monolayer was adsorbed to the surface of the Ag/Cu<sub>2</sub>O nanodendrites to generate a SERS signal. Clean electrodes were soaked in a 0.01 M ethanolic solution of MBN for 24 hours to create the monolayer.

The Raman spectroelectrochemical experiments with Ag/Cu<sub>2</sub>O/MBN were performed using a potential stepped from open circuit potential (OCP) ( $\approx 0.0 \text{V}$ ) to -0.6V in 50 mV increments, holding the potential constant while the Raman spectra were collected by mapping 10  $\mu$ m x10  $\mu$ m area with 1  $\mu$ m steps, acquiring 121 spectra at each applied potential.

## **Results and Discussion**

In situ spectroelectrochemistry experiments were performed to monitor the chemical conversion of CO<sub>2</sub> on the Ag/Cu<sub>2</sub>O electrode previously characterized spectroscopically and morphologically (Figures S2 and S3). In 0.1M Na<sub>2</sub>SO<sub>4</sub> solution, -0.4V vs Ag/AgCl was applied for 30 minutes under continuous 455 nm LED illumination. The 455 nm LED avoids interference with the Raman scattering from the 632.8 nm laser. Figure 1a shows spectra recorded from a CO<sub>2</sub>-saturated solution under LED illumination as a function of time. New peaks are observed that are not detected in the control experiments performed in a N<sub>2</sub>-saturated solution or from a CO<sub>2</sub>-saturated solution without LED illumination (Figure S4). In Figure 1a, these new bands are assigned to

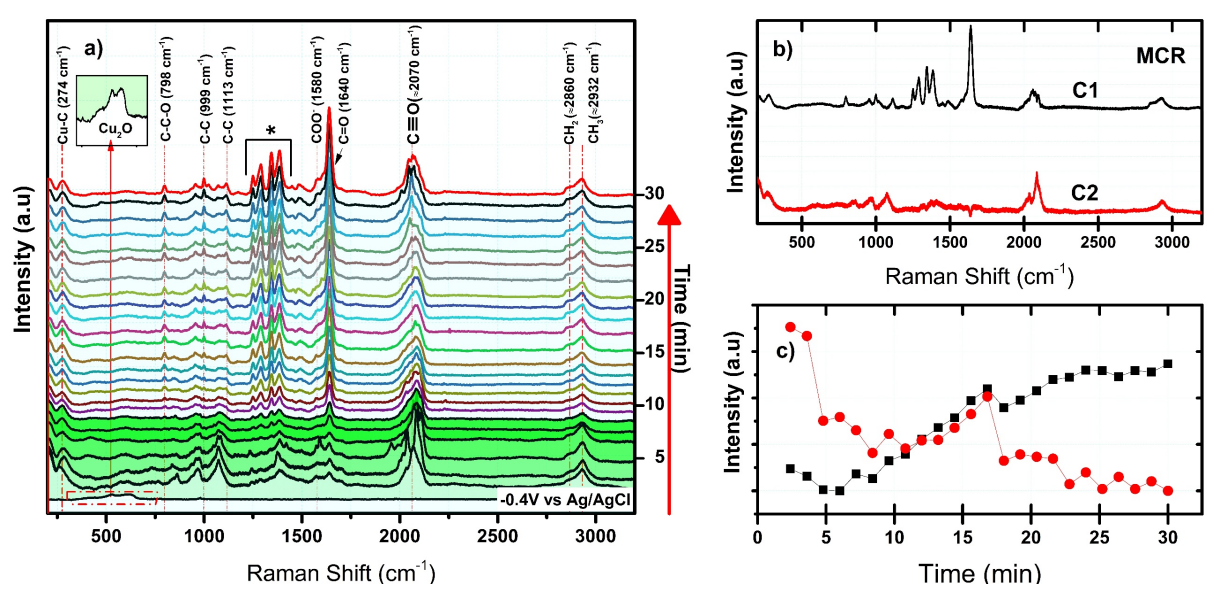


Figure 1: a) Raman spectra of  $Ag/Cu_2O$  electrodes for  $CO_2$  reduction carried out under 455 nm LED illumination and applying -0.4V vs Ag/AgCl for 30 minutes. b) MCR analysis of the spectra collected decomposed into the 2 main components. c) Intensity vs time is shown for the MCR components. The two MCR components account for > 99% of the variance in the data.

various, C-C, C-O, and C-H containing functional groups. Other bands are difficult to identify due to the close proximity between the peak frequencies, as can be seen in the region between 1200-1400 cm<sup>-1</sup> where at least 4 peaks (see \* in the figure 1a) are observed that could correspond to stretching, bending or deformation of COO-, CH<sub>2</sub> and O-CH<sub>3</sub> bonds <sup>25–27</sup>. These bands are consistent with our previous report of photoreduction of CO<sub>2</sub> to acetate on this surface. <sup>12</sup>

The time resolved spectra indicate two different reaction regimes over the course of the electrolysis. At the beginning, the bands assigned to Cu<sub>2</sub>O surface species disappear when the -0.4 V potential is applied, which suggests the rapid activation of the surface with the adsorption of CO<sub>2</sub> molecules. These bands are accompanied by broad bands in regions characteristic of C-H, C=O and CO that start to appear. At approximately 8 minutes into the electrolysis reaction, the spectrum changes and the new peaks persist until the end of the reaction, while the peaks observed in the initial reaction diminish. To clarify the changing spectral patterns, multivariant curve resolution (MCR) analysis was used to deconvolute the components of the SERS data. A two component model accounted for essentially all the variance in

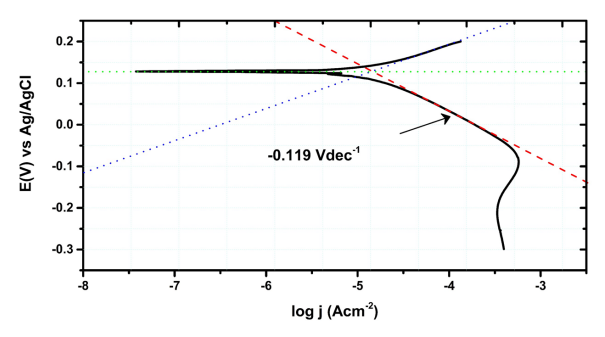
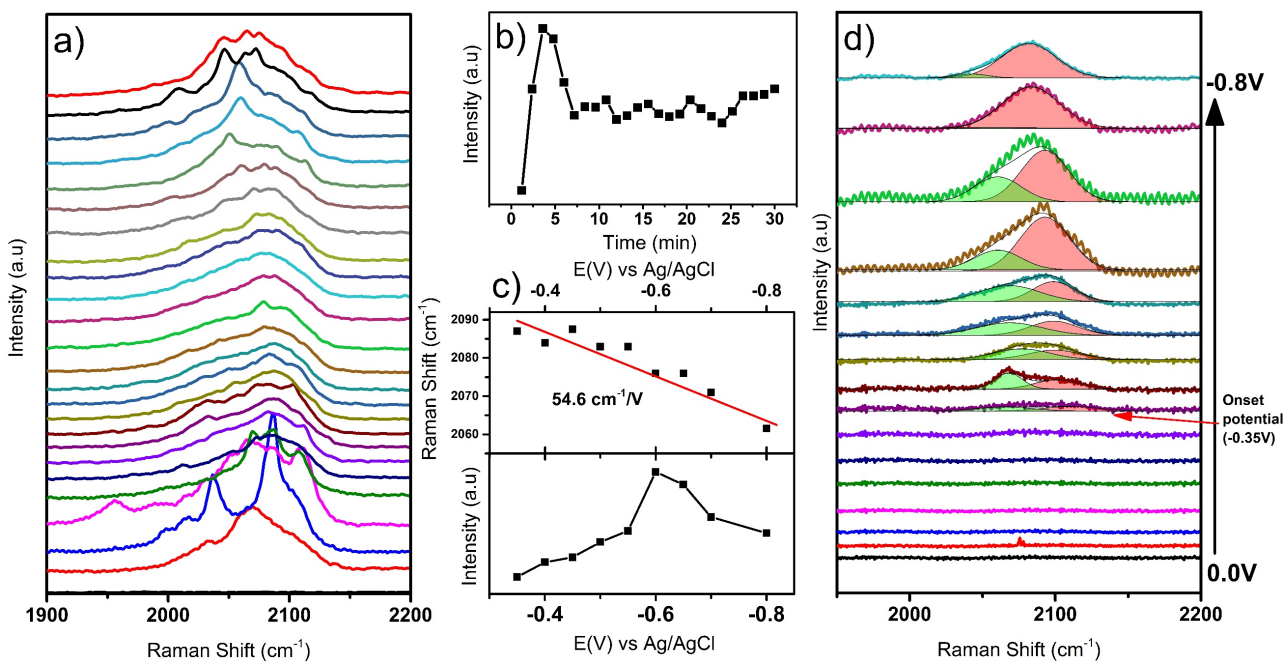


Figure 2: Tafel plot recorded for the photoelectrochemical reduction of  $CO_2$  to acetate using  $Ag/Cu_2O$  electrodes.

the data, with component 1 (C1) contributing 74.5% and component 2 (C2) accounting for 25.5% (Figure 1b). Component 1 and component 2 show different time dependent contributions to the overall signal (Figure 1c). Component 2 is dominant initially; however, component 2 diminishes and component 1 is observed to grow in intensity during the reaction. The SERS signals in Figure 1a, from the CO<sub>2</sub>-saturated solution, shows changes in peak frequency and intensity that can be used to identify reaction intermediates and to evaluate its behavior over time, enabling us to propose a reduction mechanism. The identification of these intermediates is presented below.

Anion radical \*CO<sub>2</sub>-: The carboxylate radical anion (\*CO<sub>2</sub><sup>-)</sup> has previously been detected on metallic surfaces of copper and silver. Vibrational modes at 700 and 1540 cm<sup>-1</sup> have been identified for in-plane deformation and asymmetric stretching, respectively<sup>19,26–28</sup>. These peaks are consistent with our SERS spectra (Figure. 1a), where a small peak at 698 cm<sup>-1</sup> is visible during the electrolysis time while a shoulder at 1580 cm<sup>-1</sup> can be assigned to the asymmetric stretching of \*CO<sub>2</sub>-. Contrary to what might be expected regarding the intensity of these bands, they are both weak. The SERS signals suggest that this radical anion, once adsorbed on the surface of the electrode, is rapidly reduced to form new C-C, C-O and C-H bonds. The formation of this reaction intermediate is further supported by electrochemical studies analyzing the behavior of the Tafel slope. Figure 2 shows the Tafel behavior of the Ag/Cu<sub>2</sub>O nanodrendrites under white light illumination (100 mWcm<sup>-2</sup>) in the electrochemical window from +0.2V to -0.3V vs Ag/AgCl. The cathodic Tafel slope is 119 mV dec-1, which is consistent with a rate determining step being the initial oneelectron reduction of CO2 forming the carboxylate radical anion \*CO2<sup>-</sup>.29 The agreement between the spectroscopy and Tafel plot enables us to discard others possible steps, such as the formation of carboxyl or formyloxyl species through Proton-coupled electron transfer (PCET) or through hydride transfer mechanisms.26



**Figure 3**: a) SERS spectra for the CO stretching and b) CO frequency intensity during an electrolysis of 30 minutes at -0.4V in a CO<sub>2</sub>-saturated 0.1M Na<sub>2</sub>SO<sub>4</sub> solution. c) Raman shift and CO intensity of the CO peak d) potential dependence of the CO frequency in an experiment carried out from open circuit potential (~0.0V) to -0.8V

Carbon monoxide: Using copper and oxide-derived copper electrodes, various publications have proposed that the formation and adsorption of CO is key for the formation of the C−C bond, through a dimerization reaction. This coincides with publications reporting the formation of the C₂ compounds CH₃COO⁻, CH₃CH₂OH, and C₂H₄ as products.³0-33 Our results show that during CO₂ reduction, \*C≡O appears throughout the process with an intense broad SERS band at ~2070 cm⁻¹ (Figure. 1a). Our prior report detected trace amounts of CO (g) during electrolysis.¹² The band at 2070 cm⁻¹ has been uniquely assigned to CO stretching, which, depending on the degree of adsorption, shifts to a lower frequency than for the free molecule. The adsorbed \*CO assignment is further supported by the Raman band at 280 cm⁻¹ assigned to Cu-CO frustrated rotation in our data.

Analysis of the CO band intensity over the course of the reaction (figure 3a and b) indicate that the concentration of CO on the surface increases rapidly during the first minutes of the reaction, reaching a maximum at about 5 minutes, and then decreases and to a steady state until the end of the reaction, which agrees with the MCR analysis in Figure 1, suggesting component 2 and the behavior of the spectra during the first minutes of the electrolysis reaction arise from CO<sub>2</sub> reduction to adsorbed CO on the surface. This adsorption and reduction to CO is in accordance with prior literature where of C<sub>2</sub> and C<sub>2+</sub> compounds are formed.<sup>10,34,35</sup>

The potential dependence (Figure 3c) of the CO peak indicates that this intermediate is chemisorbed onto our nanodendrite surface at a considerably higher rate than reported for metallic copper electrodes, <sup>26</sup> which we believe is a key factor in the high selectivity towards the formation of acetate. It has been reported that the selectivity in CO<sub>2</sub> reduction is highly dependent on the adsorption strength of key intermediates <sup>36,37</sup>. Deconvolution of the \*CO peak (figure

3d) shows at least two different interactions are detected on our electrode. The intensity and frequency of peaks associated with the \*CO changes as the applied potential becomes more negative. At the onset potential of -0.35 V, the \*CO band is weighted toward a low frequency component, and as the applied potential becomes increasingly negative, the intensity in the \*CO manifold shifts to higher frequency, and the low frequency component disappears. The disappearance of the low frequency \*CO band is consistent with reduction of Cu<sub>2</sub>O to Cu, and possibly the desorption of CO from the metal surface. The prevalence of this low energy peak at less negative potentials indicates the importance of Cu<sup>+</sup> in the selectivity of the reaction. The importance of stabilizing Cu+ for selective CO<sub>2</sub> reduction has been previously reported.<sup>38</sup> For example Chu et al<sup>38</sup> used a CuO-CeO<sub>2</sub> interface to stabilize Cu<sup>+</sup> and produce ethylene with a faradaic efficiency (FE) as high as 50.0% at −1.1 V vs RHE.

Carbonate: The SERS spectra show intense peaks at ~1070 cm<sup>-1</sup> (Figure 1a), previously assigned to adsorbed carbonate. This peak is almost unaffected by potential indicating that the CO<sub>3</sub><sup>2-</sup> anion is physisorbed to the surface of the nanodendrite as shown in (Figure S5). The onset potential for the appearance of the peak is -0.2V, where the surface is expected to be negatively charged. The peak position of CO<sub>3</sub><sup>2-</sup> at -0.4V is close to the peak position of dissolved CO<sub>3</sub><sup>2-</sup>,<sup>26</sup> indicating the adsorption strength is relatively weak. Detecting CO<sub>3</sub><sup>2-</sup> instead of HCO<sub>3</sub><sup>-</sup>, which is the main species in solution, indicates the local pH on the surface of the electrode is highly basic compared to the pH of the solution (pH=4.2). The combination of identifying the \*CO<sub>2</sub><sup>-</sup> radical anion as the RDS of the reduction, accompanied by the weak adsorption of CO<sub>3</sub><sup>2-</sup>, suggests CO<sub>3</sub><sup>2-</sup> does not participate in the CO<sub>2</sub> reduction observed.

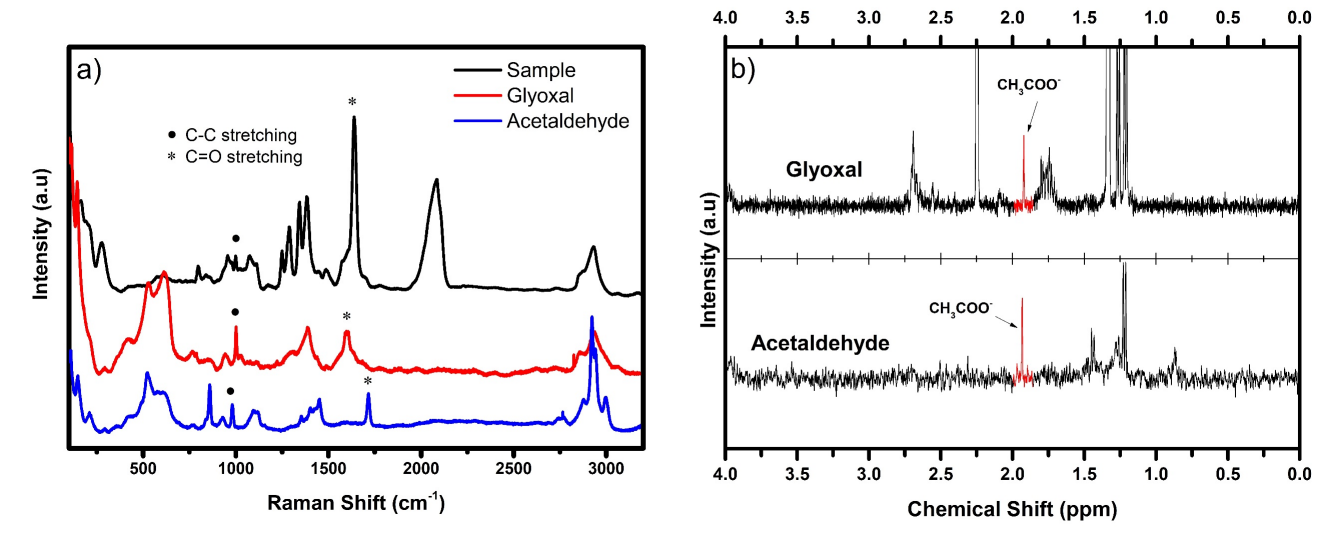


**Figure 4**: a) Average SERS spectrum of CO<sub>2</sub> reduction for 30 minutes compared with the spectra of glyoxal and acetaldehyde in 0.1M Na<sub>2</sub>SO<sub>4</sub>. b) <sup>1</sup>H NMR of glyoxal and acetaldehyde solution after electrolysis carried out at -0.4V and under light illumination. The peak assigned to acetate is highlighted in red.

C<sub>2</sub> intermediates: Prior literature of CO<sub>2</sub> reduction to C<sub>2</sub> compounds on copper surfaces has implicated glyoxal, oxalate and, acetaldehyde as possible intermediates that end up forming ethylene, ethanol, ethylene glycol, glycolaldehyde or acetate as reduction products.<sup>39</sup> In addition to \*CO<sub>2</sub>, \*CO or \*CO<sub>3</sub><sup>2-</sup>, our data shows \*C=O, CH and C-C bonds that may correspond to any of these compounds. In Figure 4a, the reference spectra of glyoxal and acetaldehyde standards show features consistent with our data. To corroborate the possible role of these intermediates, we performed the electrolysis of glyoxal and acetaldehyde containing solutions under the same conditions used for the reduction of CO<sub>2</sub> and detected acetate as a reaction product by <sup>1</sup>H NMR from both compounds (Figure 4b).

#### Light and overpotential effects on the LSPR

To further explore the relationship between the LSPR and the low overpotential to reduce  $CO_2$  we performed Raman

spectroelectrochemical measurements with the Ag/Cu<sub>2</sub>O nanodendrites analyzing the vibrational Stark shift from the MBN nitrile mode under light (455 nm LED) and dark conditions (Raman laser only). The stretch mode from MBN (~2230 cm<sup>-1</sup>) provides a probe of the local surface potential which can be affected by potential, light or both<sup>40</sup>.

Figure 5a shows the observed CN stretching frequency as a function of applied electrochemical potential from MBN adsorbed to the Ag/Cu<sub>2</sub>O nanodendrites. In dark and light conditions, as the potential becomes more negative, the CN stretch frequency is observed to decrease to lower Raman shifts with a Stark tuning coefficient of 8.1 and 2.8 cm<sup>-1</sup>/V respectively, showing the increase of the negative charge on the electrode surface which will favor electron transfer from the plasmonic material to the analyte for reduction.

Interestingly, at open circuit potential with LED illumination, the observed CN stretch is lower than in the dark

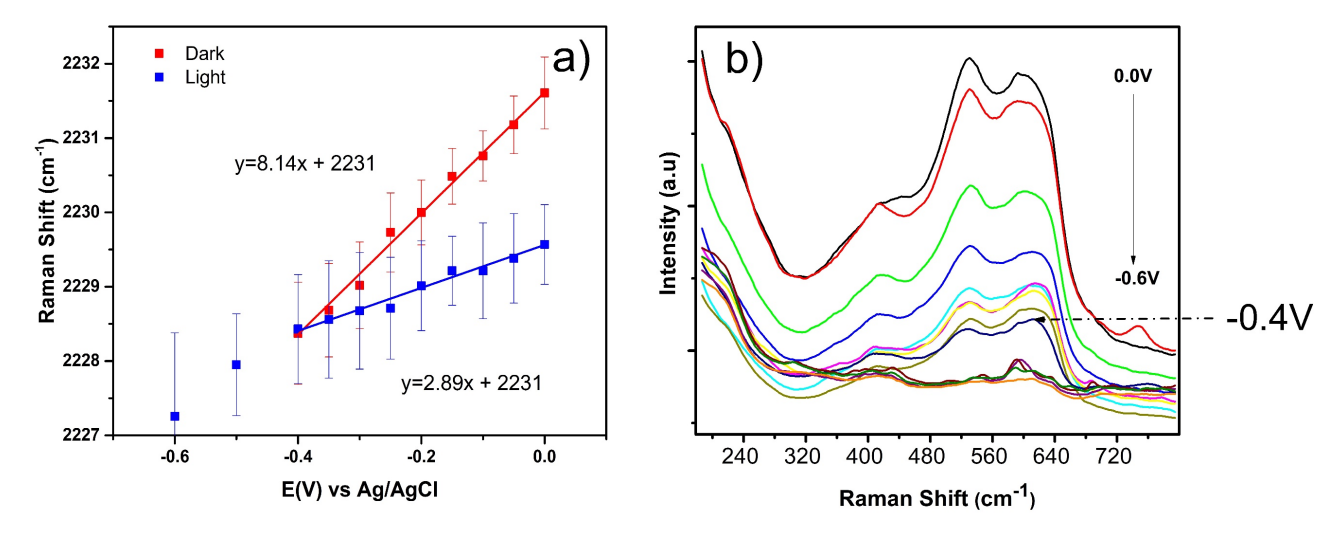


**Figure 5**: a) CN stretch frequency as a function of applied electrochemical potential under dark and continuous 455 nm LED illumination. b) Potential dependence of the Ag/Cu<sub>2</sub>O electrode during the photoelectrochemical CO<sub>2</sub> reduction

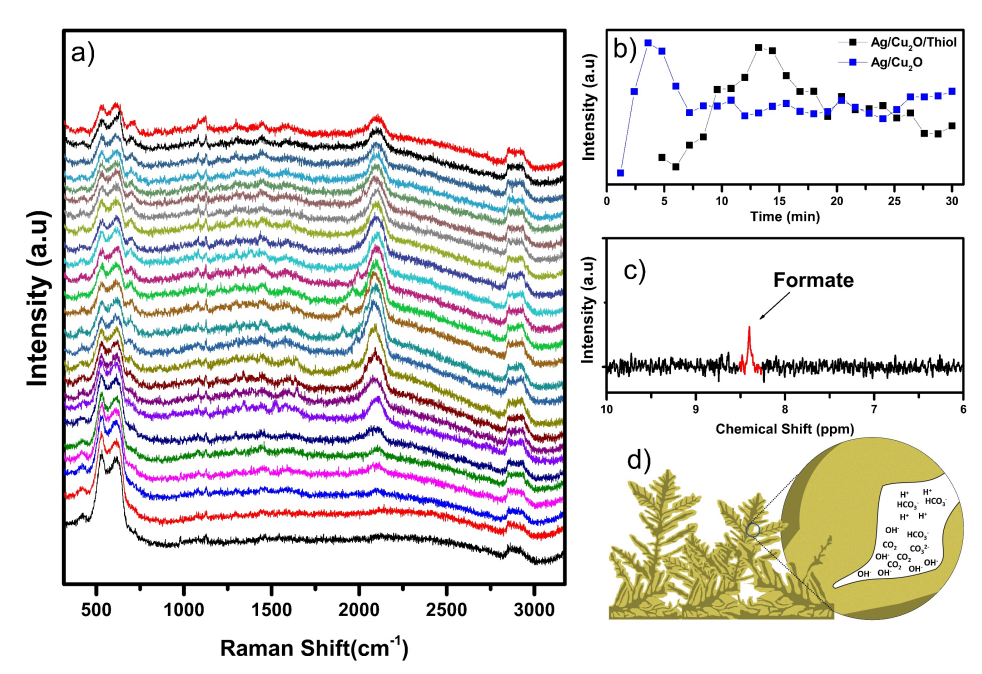


Figure 6: a) Raman spectra of  $Ag/Cu_2O/pentanethiol$  electrodes for  $CO_2$  reduction carried out under 455 LED illumination and applying -0.4V vs Ag/AgCl for 30 minutes. b) CO intensity comparison of  $Ag/Cu_2O$  with  $Ag/Cu_2O/pentanethiol$ . C) H NMR of formate peak when a  $Ag/Cu_2O/pentanethiol$  electrodes was used. d) Representative scheme of microenvironment of  $Ag/Cu_2O$  during the  $CO_2$  reduction process.

condition, indicating that the surface potential is strongly affected by LED illumination. A linear extrapolation of the nitrile frequency with applied potential with and without illumination shows an intercept near -0.4 V. After -0.4 V, the change in the nitrile frequency is the same for both light and dark conditions. Interestingly, the behavior of the stretch mode from MBN seems to be related to the CO2 reduction potential where at -0.4V acetate was detected and yet at higher potentials, the electrode is reduced to something more consistent with Cu<sup>0</sup> as shown in Figure 5b. The stability of our material is limited to a small electrochemical window that goes from open circuit potential to -0.4V. At potentials more positive than OCP, the silver nanodendrites are oxidized while at potentials more negative than -0.4V the reduction of Cu<sub>2</sub>O takes place. However, -0.4V seems to be the ideal potential for CO<sub>2</sub> reduction.

We believe that at -0.4V the Cu<sub>2</sub>O surface is partially reduced to Cu, which improves CO adsorption facilitating electronic transfer from the excited plasmon resonance. Ren et al. observed that in aqueous solution and using Cu<sub>2</sub>O that CO<sub>2</sub> reduction improves when the Cu<sub>2</sub>O is reduced to Cu<sup>0</sup> at negative potentials.<sup>41</sup> In a similar work Kas et al. investigated Cu<sub>2</sub>O with different orientation and thickness and concluded that the selectivity depends on the initial Cu<sub>2</sub>O thickness and not on the orientation<sup>42</sup> and, in agreement with Ren et al., concluded that CO2 reduction begins only after Cu2O is reduced to Cu<sup>0</sup>. In contrast to what was stated by Ren and Kas, our results indicate that Cu2O is an important material during the CO<sub>2</sub> reduction and changes in Stark tuning rate of the CN stretch under light illumination support this role of Cu<sub>2</sub>O. Another report by Kim et al indicated the importance of Cu<sub>2</sub>O for reducing CO2 using branched copper oxide activated to cuprous oxide to obtain highly selective ethylene production<sup>43</sup>. Our results indicate that at -0.4V the efficiency in reducing CO<sub>2</sub> is higher compared to other applied potentials. In addition to the presence of Cu<sub>2</sub>O on the plasmonic surface of silver, it is possible that at this -0.4 V reduction potential part of the Cu<sub>2</sub>O is reduced to copper metal in a proportion such that the material retains its initial nature but that with the presence of Cu<sup>0</sup>, the CO<sub>2</sub> adsorption is favored improving its reduction.

We note that electrolysis was performed with a white light LED, while the Raman measurements used a 455 nm LED. However, the correlation between species evident by NMR (white light) and Raman (455 nm) indicate the illumination conditions do not have a significant impact on the observed products. It was previously reported that H<sub>2</sub> photoreduction on a Cu-ternary composite material that blue LED illumination<sup>44</sup> increased the H<sub>2</sub> yield by focusing energy into the appropriate band. Further experiments may show a wavelength dependence to further improve the acetate yield.

SERS detection of C-O, C-H and C-C bonds as well as the presence of adsorbed functional groups such as \*COO-, \*CO and \*CO³2⁻, OH⁻, aid in deducing and understanding the reduction mechanism by providing chemical information about the species present at the catalytic site and hence the selectivity of the reaction. The selectivity has been correlated to the local environment of the active sites, appropriate adsorption strength³7 of the key intermediates, and LSPR excitation at interstitials or sharp edges⁴5. Wagner et al identified three aspects of the local environment that can affect reactivity: surface effects, solution interactions and three-dimensional materials,⁴6 which we will evaluate further.

**Surface effects**: It is well known that the nature of the species adsorbed on the surface of the electrode can affect the selectivity and efficiency of CO<sub>2</sub> reduction. Thus, the early

detection of \*CO is a key compound in the selectivity of the reaction. Its adsorption not only directs the reduction towards  $C_{2+}$  compounds, but also suppresses the hydrogen evolution reaction. In our results we do not detect hydrogen by Gas Chromatography (GC) or Linear Sweep Voltammetry (LSV) experiments. The current density observed in LSV with  $N_2$  is lower than in a  $CO_2$  saturated solution (Figure S6) indicating poor  $H_2$  production at the working potential.

Electrode functionalization can alter the reaction selectivity by modifying the physicochemical nature of the surface. Our SERS results in Figure 3 suggest a buildup of adsorbed CO prior to the production of C2 products. To better understand the role of the \*CO adsorbed, we functionalized the Ag/Cu<sub>2</sub>O electrode with pentanethiol to restrict lateral surface interactions, and we carried out electrolysis and Raman photoelectrochemical experiments to see the effect on the selectivity. Wakerley et al showed electrochemical CO2 reduction to C<sub>2</sub>/C<sub>3</sub> products by functionalizing Cu dendrites with 1-octadecanethiol, attaining attained a 56% Faradaic efficiency for ethylene and 17% for ethanol.<sup>47</sup> In a similar work, Baker et al showed dodecanethiol on Au nanoparticles affects the activity, selectivity, and stability of the Au nanoparticles for electrochemical carbon dioxide reduction. In particular, they showed in the presence of this surface ligand, the yield of CO increased more than 100 times compared to the polycrystalline gold electrode at an identical potential<sup>48</sup>. Figure 6a shows the Raman spectra Ag/Cu<sub>2</sub>O/pentanethiol modified electrode at -0.4V and under continuous light illumination where unlike unmodified electrodes, only the 2070 cm<sup>-1</sup> peak, attributed to CO stretching, changes over time, which indicates that there is reduction from CO2 to CO, but this intermediate does not react further to a C2 or C2+ compound. Figure 6b shows the CO intensity when the Ag/Cu<sub>2</sub>O/pentanethiol and Ag/Cu<sub>2</sub>O electrodes are compared. For the Ag/Cu<sub>2</sub>O/pentanethiol electrodes the maximum CO intensity occurs at least 10 minutes later than the Ag/Cu<sub>2</sub>O electrodes which shows that the functionalization of the electrodes with pentanethiol affects the CO<sub>2</sub> reduction.

Electrolysis at controlled potential on the pentanethiol covered surface shows a change in the detected product. Formate is produced in solution on the pentanethiol covered surface, as detected by <sup>1</sup>H NMR in Figure 6c. Formate is considered a dead end pathway in the reduction of CO<sub>2</sub>. Using a silver catalyst surface, Bohra et al. reported the adsorbed formate intermediate (\*OCHO) may react with adsorbed protons (\*H) along the reaction pathway towards CO.<sup>49</sup> In our Raman spectroelectrochemical experiments, a maximum intensity for the CO stretching is observe at ~13 minutes, after which the intensity begins to decrease(Figure 6b). The SERS detection of CO on the Ag/Cu<sub>2</sub>O/pentanethiol electrodes suggests the functionalization with thiols affects the surface diffusion of CO molecules, blocking dimerization reactions by increasing the distance between adsorbed CO moieties, and thus preventing the formation of the C-C bond that results in the formation of acetate. However, the functionalization does not seem to affect the nature of the Ag/Cu<sub>2</sub>O electrode with bands corresponding to Cu<sub>2</sub>O (figure 6a) are present throughout the electrolysis as well as the CO stretch bands

whose SERS intensity is not affected by the presence of pentanethiol. Also, the detection of formate as well as the formation of acetate with non-functionalized electrodes at low overpotential (-0.4V) is evidence that the photoelectrocatalytic activity is not interrupted, and the hot electrons generated by LSPR are still reaching the Cu<sub>2</sub>O surface to promote the reduction the CO<sub>2</sub>.

Solution interactions: In addition to the adsorbed species, the species in solution, mainly Na<sup>+</sup>, CO<sub>3</sub><sup>2</sup>-, HCO<sub>3</sub><sup>-</sup>, H<sub>2</sub>CO<sub>3</sub> and OH<sup>-</sup> ions create a unique microenvironment for the selective reduction of CO<sub>2</sub>. Na<sup>+</sup> and SO<sub>4</sub><sup>2-</sup> ions are present due to their use as the supporting electrolyte, while CO32-, HCO3- and H2CO3 arise from the acid-base equilibrium established when CO2 is dissolved in water. The detection of CO<sub>3</sub><sup>2</sup>- over HCO<sub>3</sub>- and H<sub>2</sub>CO<sub>3</sub> is an indicator of a highly basic microenvironment which impacts pH-sensitive reactions on the surface, but the low adsorption energy indicates the presence of CO<sub>3</sub><sup>2-</sup> does not affect the CO<sub>2</sub> reduction. The OHions arise from the CO<sub>2</sub> reduction process or water splitting. Acetate production generates 7 OH- anions for every 2 CO<sub>2</sub> molecules reduced, while water splitting forms 2 OH- for every 2 H<sub>2</sub>O molecules increasing the local alkalinity. The effect of pH on selectivity towards C<sub>2</sub> and C<sub>2+</sub> compounds is a widely discussed issue. Lijima et al<sup>50</sup> reported the local pH affects the catalytic activity, indicating that the OH layer attracts \*CO molecules closer to each other while reducing them to C2 and C<sub>2+</sub> products. This observation agrees with Liu et al who reported C2 products are favored from CO2 reduction under alkaline conditions on Cu electrodes.51

Three-dimensional materials: The morphology of the Ag/Cu<sub>2</sub>O nanodendrite shows a complex branching with surface roughness forming diffusion gradients that can impact the local alkalinity and the acetate selectively as is shown in the scheme of the Figure 6d. The branched structure may promote a basic microenvironment that differs from the bulk of the solution. In this microenvironment, the production of acetate is thermodynamically favored with respect to ethanol, ethylene, or ethane, whose corresponding standard redox potentials vs RHE are -0.65, -0.74, -0.74 and -0.68, respectively.9 Most of the prior research using copper or copper derivatives report good efficiencies for the production of ethanol, ethylene, or ethane over acetate, indicating that the CO<sub>2</sub> reduction to acetate is kinetically unfavorable with copper electrodes. However, as we have previously described, our material reduces CO2 to acetate with high efficiency at a very low overpotential. We believe the branch structure not only generates the LSPR and energetic charge carriers, but also favors an ideal microenvironment for the formation of acetate. Other dendritic materials have been explored for CO2 reduction. Scholten et al fabricated dendritic Cu electrocatalysts improving the selectivity toward ethylene and ethanol establishing a strong structure/chemical stateselectivity correlation in CO<sub>2</sub> reduction.<sup>49</sup> Similarly Urbain et al fabricated a highly selective silver dendrite catalyst to reduce CO2 to CO and attributed the activity to the large surface area of the nanodendrites<sup>52</sup>.

# Effect of the isotope exchange on SERS spectra

To further validate the observed intermediates, we made SERS measurements substituting the CO<sub>2</sub> and the solvent for

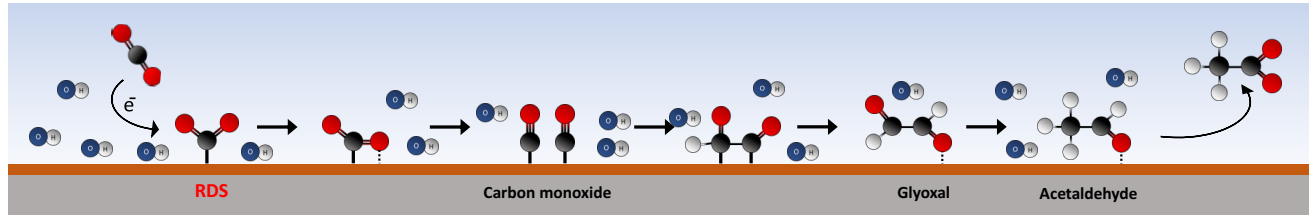


Figure 7: Proposed mechanism for the reduction of CO<sub>2</sub> to Acetate on Ag/Cu<sub>2</sub>O electrodes

<sup>13</sup>CO<sub>2</sub> and D<sub>2</sub>O respectively. For D<sub>2</sub>O/H<sub>2</sub>O isotope exchange experiments the peaks at 1250, 1343 and 1487 cm<sup>-1</sup> were redshifted (Figure S7a), which corroborates that the chemical bonds involve at least one C-H bond that affects the observed vibrational mode. These peaks correspond to C-H bond coming from CH deformation and CH<sub>2</sub>, CH<sub>3</sub> asymmetric stretching, respectively, based on prior reports.<sup>27</sup> <sup>13</sup>C isotopic substitution resulted in the peaks at 1640 and 2086 cm<sup>-1</sup> being red-shifted to 1593 and 2073 cm<sup>-1</sup>, respectively (Figure S7b). The Stark the CO shift observed from these peaks with applied potential showed the same trend (Figure 3d), which is evidence that the chemical bond is related to a carbon atom from the carbonyl (C=O) and CO (C=O) group. <sup>13</sup>C/<sup>12</sup>C isotope exchange effect also allowed us to eliminate possible organic contamination coming from the electrode preparation or the electrochemical cell.

#### Mechanism and discussion

The photoelectrocatalytic activity of  $Ag/Cu_2O$  nanodendrites generates acetate as the major product and small concentrations of CO. These products, the *in situ* Raman spectroelectrochemistry studies, and Tafel analysis support the mechanism for the photoelectrochemical reduction of  $CO_2$  to acetate shown in Figure 7.

First, the Tafel slope values indicate the dissolved CO2 is adsorbed on the electrode and reduced to the radical anion \*CO<sub>2</sub>- through a single electron transfer from the electrode to the CO<sub>2</sub>. The activation of CO<sub>2</sub> is an energetically unfavorable process with a thermodynamic reduction potential of -1.9V vs NHE,<sup>18</sup> though well within the energy range expected for a hot electron generated by the LED illumination. The partial reduction to \*CO<sub>2</sub>- on the dendritic cuprous oxide surface is improved by the generation of hot-electrons from the underlying silver that increase the available electrons on the conduction band of the semiconductor which decreases the reduction potential to -0.4V vs Ag/AgCl. The specific -0.4 V appears to be related to the oxidation state of the Cu, where the reaction occurs. The stark-shift and Raman data in Figure 5 indicate plasmon modulation of the Cu<sub>2</sub>O and Cu composition at this potential; however, the reaction is not observed on Cu surfaces without plasmonic assistance, indicating Cu<sub>2</sub>O is the important surface species. We infer that Cu may promote adsorption of the initial CO2 species. In the next step, this radical is reduced to \*CO adsorbed to the surface to be further reduced to C<sub>2+</sub> products through C-C coupling.

The \*CO<sub>2</sub> to \*CO pathway has been studied extensively and various stabilization mechanisms have been proposed, for example some works have shown that the \*CO<sub>2</sub>- is stabilized by a single proton transfer from water, and then through a proton-electron transfer is reduced to \*CO.<sup>53,54</sup> Another

pathway proposed by Sheng and collaborators,<sup>55</sup> the \*CO<sub>2</sub> is reduced to \*CO through a single electron transfer of a \*CO<sub>2</sub> dimer radical anion to convert it to \*CO and CO<sub>3</sub><sup>2</sup>. Other works indicate that the pathway from CO<sub>2</sub> towards the intermediate \*CO strongly depends on the excitation wavelength and the nature of the catalyst, where recent research<sup>56</sup> suggests that the activation and division of the CO<sub>2</sub> molecule depends on hot electrons produced from the decay of and that the strong reduction of this molecule from these hot electrons is accompanied by its stabilization through the surface (S) and solvent molecules (Ln) as shown in the following equation:

$$(S*CO_2)^-Ln + hv \rightarrow (S*O)^-Ln*CO$$

Where the \*CO<sub>2</sub><sup>-</sup> dissociation takes place on the excited state potential energy surface, which may yield an adsorbed \*CO molecule. The formation of adsorbed \*CO agrees with our in situ time-resolved experiments, where we observe a rapid increase in \*CO during the first minutes of electrolysis that then persists during the entire time the experiment is carried out. It has been well documented that the increase of CO on the surface of the electrode favors the dimerization, 3,50,57 giving way to the formation of C2 compounds. Interestingly, in our in situ experiments when CO intensity remain stable, the peaks at 1640 and 1384 cm<sup>-1</sup> begins to raise. Then 2 \*CO molecules dimerize to form a C-C coupling favored by an increased local pH due to CO<sub>2</sub> or H<sub>2</sub>O reduction as previously discussed. This coupling gives rise to oxygenated intermediaries through proton-electron transfer. The existence of these new intermediates is clearly detected by the identification of new Raman peaks at 797 cm<sup>-1</sup> assigned to C-CO stretching, and two peaks at 997 and 1112 cm<sup>-1</sup> both assigned for C-C stretching (figure 1a). Glyoxal and acetaldehyde appear to be possible oxygenated intermediates supported by the in situ SERS spectra and H NMR experiments. We detect acetate using glyoxal and acetaldehyde as starting compounds instead of CO<sub>2</sub>, indicating that glyoxal and acetaldehyde are intermediates along pathway to form acetate as the majority product. It has been shown that glyoxal can be reduced to acetaldehyde at low overpotential, and at higher overpotential that the acetaldehyde can be reduced to ethanol.<sup>39</sup> Our results show no evidence of ethanol, likely due to the low overpotential necessary for the reduction and the rapid e-/h+ transfer from the bulk electrode to the surface to react with the CO2 molecule. The change in observed products with the functionalization of the electrode with pentanethiol supports lateral interactions on the copper surface are important to enable \*CO molecules to dimerize and be reduced to acetate. When these active sites are blocked, the selectivity changes toward the formation of C1 products. The physical and nature of the electrode does not change despite the formation of

formate instead of acetate. It is worth noting that the overpotential is still low for the  $CO_2$  reduction toward formate, which could extend the use of this type of electrodes for the reduction of  $CO_2$  towards other products.

In summary, the increased efficiency on our electrode arises from the synergistic properties of silver dendrites (hot electron generation) while presenting a thin layer of copper oxide to mediate adsorption and reactivity of the adsorbed CO. The high efficiency (54%), low overpotential (-0.4V vs Ag/AgCl) and selectivity towards acetate formation derives from the physical-chemical nature of our electrodes that create the ideal microenvironment for efficient and selective CO<sub>2</sub> reduction. Importantly, prior reports of acetate production efficiency do not exceed 15% with copper electrodes or copper derivatives.<sup>58</sup>

## **Conclusions**

In conclusion, electrochemical and spectroelectrochemical methods enable the mechanism by which CO2 is photoelectrochemically reduced to acetate on dendritic nanomaterials with plasmonic and semiconductor properties to be elucidated. The SERS signal produced by our material allowed us to identify possible intermediates to deduce the mechanism by which CO2 was transformed into acetate, or formate if pentanethiol is incorporated. The mechanism proposes \*CO<sub>2</sub><sup>-</sup> as the slowest step in the reduction process. The fast CO increase and the strong adsorption on the electrode surface is evidence that acetate production depends on the formation of this intermediate, whose increase is favored by the basic microenvironment of the surface. The preference for acetate over ethanol is explained by several aspects: the nature of the electrode (plasmonic and semiconductor material) modulating adsorption and reactivity, a highly basic local microenvironment, and the large area provided by the nanodendrites. The basic pH of the local microenvironment arises from either CO<sub>2</sub> or H<sub>2</sub>O reduction on the electrode surface. This highly basic condition is favored by the branched structure of the nanodendrite which allows the accumulation of OH- ions in the corners and edges of the nanodendrites, decreasing the thickness of the diffusion layer, and favoring mass transport for CO<sub>2</sub> electrolysis. We believe this basic microenvironment favors the lateral interaction between CO molecules to form acetate as the final product. These all contribute to the selectivity for acetate when an overpotential, as low as the thermodynamic reduction potential, is applied and the plasmon resonance is photoexcited (-0.4V vs Ag / AgCl). Our studies on this photocatalysist show an efficient and selective system towards the reduction of CO2 to acetate and suggest that lateral interactions on the electrode surface are important for the formation of C<sub>2+</sub> products. Our results illuminate the identity of key intermediates that may impact the formation of other products; either by controlling the dendrites and Cu<sub>2</sub>O, or by controlling the applied potential and illumination to activate the material. This understanding may enable not only acetate production but also the selective reduction towards CO or more complex CO2 reduction products. This improved mechanistic understanding of CO<sub>2</sub> photoelectroreduction with plasmonic and semiconductor materials enables efficient and

selective production of high added value compounds such as acetate from CO<sub>2</sub> under low cost and environmentally friendly environmental conditions.

# Supporting Information

Figures S1-S7 providing characterization, additional control experiments, and additional details are provided.

# Acknowledgment

This work was supported by the Ohio State University and the National Science Foundation through award CHE-2107791.

# References

- (1) Von Schneidemesser, E.; Monks, P. S.; Allan, J. D.; Bruhwiler, L.; Forster, P.; Fowler, D.; Lauer, A.; Morgan, W. T.; Paasonen, P.; Righi, M.; Sindelarova, K.; Sutton, M. A. Chemistry and the Linkages between Air Quality and Climate Change. *Chem. Rev.* 2015, 115 (10), 3856–3897.
- (2) Kumaravel, V.; Bartlett, J.; Pillai, S. C. Photoelectrochemical Conversion of Carbon Dioxide (CO<sub>2</sub>) into Fuels and Value-Added Products. ACS Energy Lett. 2020, 486–519.
- (3) Zhu, Q.; Sun, X.; Yang, D.; Ma, J.; Kang, X.; Zheng, L.; Zhang, J.; Wu, Z.; Han, B. Carbon Dioxide Electroreduction to C2 Products over Copper-Cuprous Oxide Derived from Electrosynthesized Copper Complex. Nat. Commun. 2019, 10, 3851.
- (4) Gurudayal; Bullock, J.; Srankó, D. F.; Towle, C. M.; Lum, Y.; Hettick, M.; Scott, M. C.; Javey, A.; Ager, J. Efficient Solar-Driven Electrochemical CO<sub>2</sub> Reduction to Hydrocarbons and Oxygenates. *Energy Environ. Sci.* 2017, 10 (10), 2222–2230.
- (5) Hori, Y.; Kikuchi, K.; Murata, A.; Suzuki, S. Production of Methane and Ethylene in Electrochemical Reduction of Carbon Dioxide At Copper Electrode in Aqueous Hydrogencarbonate Solution. Chem. Lett. 1986, 15 (6), 897–898.
- (6) Hori, Y.; Murata, A.; Takahashi, R. Formation of Hydrocarbons in the Electrochemical Reduction of Carbon Dioxide at a Copper Electrode in Aqueous Solution. J. Chem. Soc. Faraday Trans. 1 Phys. Chem. Condens. Phases 1989, 85 (8), 2309–2326.
- (7) Kuhl, K. P.; Cave, E. R.; Abram, D. N.; Jaramillo, T. F. New Insights into the Electrochemical Reduction of Carbon Dioxide on Metallic Copper Surfaces. *Energy Environ. Sci.* 2012, 5, 7050–7059.
- (8) Wu, J.; Ma, S.; Sun, J.; Gold, J. I.; Tiwary, C.; Kim, B.; Zhu, L.; Chopra, N.; Odeh, I. N.; Vajtai, R.; Yu, A. Z.; Luo, R.; Lou, J.; Ding, G.; Kenis, P. J. A.; Ajayan, P. M. A Metal-Free Electrocatalyst for Carbon Dioxide Reduction to Multi-Carbon Hydrocarbons and Oxygenates. Nat. Commun. 2016, 7, 1–6.
- (9) Fan, L.; Xia, C.; Yang, F.; Wang, J.; Wang, H.; Lu, Y. Strategies in Catalysts and Electrolyzer Design for Electrochemical CO<sub>2</sub> Reduction toward C<sub>2+</sub> Products. Sci. Adv. 2020, 6 (8), 1–18.
- (10) Huang, Y.; Handoko, A. D.; Hirunsit, P.; Yeo, B. S.

- Electrochemical Reduction of CO<sub>2</sub> Using Copper Single-Crystal Surfaces: Effects of CO<sub>\*</sub> Coverage on the Selective Formation of Ethylene. *ACS Catal.* **2017**, 7 (3), 1749–1756.
- (11) Ooka, H.; Figueiredo, M. C.; Koper, M. T. M. Competition between Hydrogen Evolution and Carbon Dioxide Reduction on Copper Electrodes in Mildly Acidic Media. *Langmuir* **2017**, *33* (37), 9307–9313.
- (12) Landaeta, E.; Masitas, R. A.; Clarke, T. B.; Rafacz, S.; Nelson, D. A.; Isaacs, M.; Schultz, Z. D. Copper-Oxide-Coated Silver Nanodendrites for Photoelectrocatalytic CO<sub>2</sub> Reduction to Acetate at Low Overpotential. ACS Appl. Nano Mater. 2020, 3 (4), 3478–3486.
- (13) Zhang, Y.; He, S.; Guo, W.; Hu, Y.; Huang, J.; R. Mulcahy, J.; David Wei, W. Surface-Plasmon-Driven Hot Electron Photochemistry. *Chem. Rev.* 2017, 118 (6), 2927–2954.
- (14) Aslam, U.; Rao, V. G.; Chavez, S.; Linic, S. Catalytic Conversion of Solar to Chemical Energy on Plasmonic Metal Nanostructures. *Nat. Catal.* **2018**, *1* (9), 656–665.
- (15) Cortés, E.; V. Besteiro, L.; Alabastri, A.; Baldi, A.; Tagliabue, G.; Demetriadou, A.; Narang, P. Challenges in Plasmonic Catalysis. ACS Nano 2020, 14 (12), 16202–16219.
- (16) Wilson, A. J.; Mohan, V.; Jain, P. K. Mechanistic Understanding of Plasmon-Enhanced Electrochemistry. *J. Phys. Chem. C* **2019**, 29360–29369.
- (17) Zeng, X.; Choi, S. M.; Bai, Y.; Jang, M. J.; Yu, R.; Cho, H. S.; Kim, C. H.; Myung, N. V.; Yin, Y. Plasmon-Enhanced Oxygen Evolution Catalyzed by Fe2N-Embedded TiOxNy Nanoshells. ACS Appl. Energy Mater. 2020, 3 (1), 146–151.
- (18) Habisreutinger, S. N.; Schmidt-Mende, L.; Stolarczyk, J. K. Photocatalytic Reduction of CO<sub>2</sub> on TiO<sub>2</sub> and Other Semiconductors. *Angew. Chemie Int. Ed.* **2013**, 52, 7372–7408.
- (19) Heidary, N.; Ly, K. H.; Kornienko, N. Probing CO<sub>2</sub> Conversion Chemistry on Nanostructured Surfaces with Operando Vibrational Spectroscopy. *Nano Lett.* 2019, 19 (8), 4817–4826.
- (20) Pilot, R.; Signorini, R.; Durante, C.; Orian, L.; Bhamidipati, M.; Fabris, L. A Review on Surface-Enhanced Raman Scattering. *Biosensors* **2019**, *9* (2), 57.
- (21) Kumari, G.; Zhang, X.; Devasia, D.; Heo, J.; Jain, P. K. Watching Visible Light-Driven CO<sub>2</sub> Reduction on a Plasmonic Nanoparticle Catalyst. *ACS Nano* **2018**, 12 (8), 8330–8340.
- (22) Gao, J.; Zhang, H.; Guo, X.; Luo, J.; Zakeeruddin, S. M.; Ren, D.; Grätzel, M. Selective C-C Coupling in Carbon Dioxide Electroreduction via Efficient Spillover of Intermediates As Supported by Operando Raman Spectroscopy. J. Am. Chem. Soc. 2019, 141 (47), 18704–18714.
- (23) Zhao, M.; Gu, Y.; Chen, P.; Xin, Z.; Zhu, H.; Wang, B.; Zhu, K.; Yan, S.; Zou, Z. Highly Selective Electrochemical CO<sub>2</sub> Reduction to CO Using a Redox-Active Couple on Low-Crystallinity Mesoporous ZnGa<sub>2</sub>O<sub>4</sub> Catalyst. J. Mater. Chem. A 2019, 7 (15), 9316–9323.
- (24) Gu, Y. e.; Su, X.; Du, Y.; Wang, C. Preparation of Flower-like Cu<sub>2</sub>O Nanoparticles by Pulse

- Electrodeposition and Their Electrocatalytic Application. *Appl. Surf. Sci.* **2010**, *256*, 5862–5866.
- (25) Chen, J.; Li, J.; Xu, L.; Hong, W.; Yang, Y.; Chen, X. The Glass-Transition Temperature of Supported PMMA Thin Films with Hydrogen Bond/Plasmonic Interface. *Polymers (Basel)*. **2019**, *11* (4), 601.
- (26) Chernyshova, I. V.; Somasundaran, P.; Ponnurangam, S. On the Origin of the Elusive First Intermediate of CO<sub>2</sub> Electroreduction. *Proc. Natl. Acad. Sci. U. S. A.* **2018**, *115* (40), E9261–E9270.
- (27) Shan, W.; Liu, R.; Zhao, H.; He, Z.; Lai, Y.; Li, S.; He, G.; Liu, J. In Situ Surface-Enhanced Raman Spectroscopic Evidence on the Origin of Selectivity in CO<sub>2</sub> Electrocatalytic Reduction. ACS Nano 2020, 14 (9), 11363–11372.
- (28) Jiang, S.; Klingan, K.; Pasquini, C.; Dau, H. New Aspects of Operando Raman Spectroscopy Applied to Electrochemical CO<sub>2</sub> Reduction on Cu Foams. J. Chem. Phys. 2019, 150 (4), 041718.
- (29) Qiao, J.; Liu, Y.; Zhang, J. Electrode Kinetics of CO Electroreduction. In Electrochemical Reduction of Carbon Dioxide, Fundamentals and Technologies CRC; 2016; pp 103–154
- (30) Ferreira, J.; Genovese, C.; Tavella, F.; Ampelli, C.; Boldrin Zanoni, M. V.; Centi, G.; Perathoner, S. CO<sub>2</sub> Reduction of Hybrid Cu<sub>2</sub>O–Cu/Gas Diffusion Layer Electrodes and Their Integration in a Cu-Based Photoelectrocatalytic Cell. *ChemSusChem* **2019**, *12* (18), 4274–4284.
- (31) Wang, Y.; Wang, D.; Dares, C. J.; Marquard, S. L.; Sheridan, M. V.; Meyer, T. J. CO<sub>2</sub> Reduction to Acetate in Mixtures of Ultrasmall (Cu)<sub>n</sub>,(Ag)<sub>m</sub> Bimetallic Nanoparticles. *Proc. Natl. Acad. Sci. U. S. A.* **2017**, *115* (2), 278–283.
- (32) Luc, W.; Fu, X.; Shi, J.; Lv, J. J.; Jouny, M.; Ko, B. H.; Xu, Y.; Tu, Q.; Hu, X.; Wu, J.; Yue, Q.; Liu, Y.; Jiao, F.; Kang, Y. Two-Dimensional Copper Nanosheets for Electrochemical Reduction of Carbon Monoxide to Acetate. *Nat. Catal.* **2019**, *2* (5), 423–430.
- (33) Sun, S.; Watanabe, M.; Wu, J.; An, Q.; Ishihara, T. Ultrathin WO<sub>3</sub>·0.33H<sub>2</sub>O Nanotubes for CO<sub>2</sub> Photoreduction to Acetate with High Selectivity. *J. Am. Chem. Soc.* **2018**, *140* (20), 6474–6482.
- (34) Zhan, C.; Dattila, F.; Rettenmaier, C.; Bergmann, A.; Kühl, S.; García-Muelas, R.; López, N.; Roldan Cuenya, B. Revealing the CO Coverage-Driven C-C Coupling Mechanism for Electrochemical CO<sub>2</sub> Reduction on Cu<sub>2</sub>O Nanocubesvia OperandoRaman Spectroscopy. ACS Catal. 2021, 11 (13), 7694–7701.
- (35) Nitopi, S.; Bertheussen, E.; Scott, S. B.; Liu, X.; Engstfeld, A. K.; Horch, S.; Seger, B.; Stephens, I. E. L.; Chan, K.; Hahn, C.; Nørskov, J. K.; Jaramillo, T. F.; Chorkendorff, I. Progress and Perspectives of Electrochemical CO<sub>2</sub> Reduction on Copper in Aqueous Electrolyte. *Chem. Rev.* **2019**, *119* (12), 7610–7672.
- (36) Chen, Z.; Gao, M. R.; Duan, N.; Zhang, J.; Zhang, Y. Q.; Fan, T.; Zhang, J.; Dong, Y.; Li, J.; Liu, Q.; Yi, X.; Luo, J. L. Tuning Adsorption Strength of CO<sub>2</sub> and Its Intermediates on Tin Oxide-Based Electrocatalyst for Efficient CO<sub>2</sub> Reduction towards Carbonaceous Products. *Appl. Catal. B Environ.* **2020**, *277* (May), 119252.
- (37) Guo, F.; Liu, B.; Liu, M.; Xia, Y.; Wang, T.; Hu, W.;

- Fyffe, P.; Tian, L.; Chen, X. Selective Electrocatalytic CO<sub>2</sub> Reduction to Acetate on Polymeric Cu-L (L = Pyridinic N and Carbonyl Group) Complex CoreShell Microspheres. *Green Chem.* **2021**, *23* (14), 5129–5137.
- (38) Chu, S.; Yan, X.; Choi, C.; Hong, S.; Robertson, A. W.; Masa, J.; Han, B.; Jung, Y.; Sun, Z. Stabilization of Cu+by Tuning a CuO-CeO<sub>2</sub> Interface for Selective Electrochemical CO<sub>2</sub> Reduction to Ethylene. *Green Chem.* **2020**, *22* (19), 6540–6546.
- (39) Garza, A. J.; Bell, A. T.; Head-Gordon, M. Mechanism of CO<sub>2</sub> Reduction at Copper Surfaces: Pathways to C<sub>2</sub> Products. *ACS Catal.* **2018**, *8* (2), 1490–1499.
- (40) Kwasnieski, D. T.; Wang, H.; Schultz, Z. D. Alkyl-Nitrile Adlayers as Probes of Plasmonically Induced Electric Fields. *Chem. Sci.* **2015**, *6* (8), 4484–4494.
- (41) Ren, D.; Wong, N. T.; Handoko, A. D.; Huang, Y.; Yeo, B. S. Mechanistic Insights into the Enhanced Activity and Stability of Agglomerated Cu Nanocrystals for the Electrochemical Reduction of Carbon Dioxide to N-Propanol. *J. Phys. Chem. Lett.* **2016**, *7* (1), 20–24.
- (42) Kas, R.; Kortlever, R.; Milbrat, A.; Koper, M. T. M.; Mul, G.; Baltrusaitis, J. Electrochemical CO<sub>2</sub> Reduction on Cu<sub>2</sub>O-Derived Copper Nanoparticles: Controlling the Catalytic Selectivity of Hydrocarbons. Phys. Chem. Chem. Phys. 2014, 16 (24), 12194–12201.
- (43) Kim, J.; Choi, W.; Park, J. W.; Kim, C.; Kim, M.; Song, H. Branched Copper Oxide Nanoparticles Induce Highly Selective Ethylene Production by Electrochemical Carbon Dioxide Reduction. *J. Am. Chem. Soc.* **2019**, *141* (17), 6986–6994.
- (44) Chang, Y. C.; Chiao, Y. C.; Fun, Y. X. Cu2O/CuS/ZnS Nanocomposite Boosts Blue LED-Light-Driven Photocatalytic Hydrogen Evolution. *Catalysts* **2022**, *12* (9), 1035.
- (45) Hossain, M. K.; Kitahama, Y.; Huang, G. G.; Han, X.; Ozaki, Y. Surface-Enhanced Raman Scattering: Realization of Localized Surface Plasmon Resonance Using Unique Substrates and Methods. *Anal. Bioanal. Chem.* **2009**, *394* (7), 1747–1760.
- (46) Wagner, A.; Sahm, C. D.; Reisner, E. Towards Molecular Understanding of Local Chemical Environment Effects in Electro- and Photocatalytic CO<sub>2</sub> Reduction. *Nat. Catal.* **2020**, *3* (10), 775–786.
- (47) Wakerley, D.; Lamaison, S.; Ozanam, F.; Menguy, N.; Mercier, D.; Marcus, P.; Fontecave, M.; Mougel, V. Bio-Inspired Hydrophobicity Promotes CO<sub>2</sub> Reduction on a Cu Surface. *Nat. Mater.* **2019**, *18* (11), 1222–1227.
- (48) Shang, H.; Wallentine, S. K.; Hofmann, D. M.; Zhu, Q.; Murphy, C. J.; Baker, L. R. Effect of Surface Ligands on Gold Nanocatalysts for CO<sub>2</sub> Reduction.

- Chem. Sci. 2020, 11 (45), 12298–12306.
- (49) Bohra, D.; Ledezma-Yanez, I.; Li, G.; de Jong, W.; Pidko, E. A.; Smith, W. A. Lateral Adsorbate Interactions Inhibit HCOO While Promoting CO Selectivity for CO<sub>2</sub> Electrocatalysis on Silver. *Angew. Chemie Int. Ed.* **2019**, *58* (5), 1345–1349.
- (50) Iijima, G.; Inomata, T.; Yamaguchi, H.; Ito, M.; Masuda, H. Role of a Hydroxide Layer on Cu Electrodes in Electrochemical CO<sub>2</sub> Reduction. *ACS Catal.* **2019**, *9* (7), 6305–6319.
- (51) Liu, X.; Schlexer, P.; Xiao, J.; Ji, Y.; Wang, L.; Sandberg, R. B.; Tang, M.; Brown, K. S.; Peng, H.; Ringe, S.; Hahn, C.; Jaramillo, T. F.; Nørskov, J. K.; Chan, K. PH Effects on the Electrochemical Reduction of CO<sub>2</sub> towards C<sub>2</sub> Products on Stepped Copper. Nat. Commun. 2019, 10 (1), 1–10.
- (52) Tang, P.; Carretero, N. M.; Andreu, T.; Arbiol, J.; Morante, J. R. Tailoring Copper Foam with Silver Dendrite Catalysts for Highly Selective Carbon Dioxide Conversion into Carbon Monoxide. ACS Appl. Mater. Interfaces 2018, 10, 43650–43660.
- (53) Peterson, A. A.; Abild-Pedersen, F.; Studt, F.; Rossmeisl, J.; Nørskov, J. K. How Copper Catalyzes the Electroreduction of Carbon Dioxide into Hydrocarbon Fuels. *Energy Environ. Sci.* **2010**, *3* (9), 1311–1315.
- (54) Kortlever, R.; Shen, J.; Schouten, K. J. P.; Calle-Vallejo, F.; Koper, M. T. M. Catalysts and Reaction Pathways for the Electrochemical Reduction of Carbon Dioxide. J. Phys. Chem. Lett. 2015, 6 (20), 4073–4082
- (55) Sheng, H.; Oh, M. H.; Osowiecki, W. T.; Kim, W.; Alivisatos, A. P.; Frei, H. Carbon Dioxide Dimer Radical Anion as Surface Intermediate of Photoinduced CO<sub>2</sub> Reduction at Aqueous Cu and CdSe Nanoparticle Catalysts by Rapid-Scan FT-IR Spectroscopy. J. Am. Chem. Soc. 2018, 140 (12), 4363– 4371.
- (56) Habteyes, T. G. Anions as Intermediates in Plasmon Enhanced Photocatalytic Reactions. *J. Phys. Chem. C* **2020**, *124*, 26554–26564.
- (57) Huang, Y.; Ong, C. W.; Yeo, B. S. Effects of Electrolyte Anions on the Reduction of Carbon Dioxide to Ethylene and Ethanol on Copper (100) and (111) Surfaces. *ChemSusChem* 2018, 11 (18), 3299– 3306.
- (58) Clark, E. L.; Hahn, C.; Jaramillo, T. F.; Bell, A. T. Electrochemical CO<sub>2</sub> Reduction over Compressively Strained CuAg Surface Alloys with Enhanced Multi-Carbon Oxygenate Selectivity. J. Am. Chem. Soc. 2017, 139 (44), 15848–15857.